Stoichiometry of the KCNQ1 – KCNE1 ion channel complex

Koichi Nakajo[a,b,c], Maximilian H. Ulbrich[c,1], Yoshihiro Kubo[a,b], and Ehud Y. Isacoff[c,d,e,2]

[a]Division of Biophysics and Neurobiology, National Institute for Physiological Sciences, Okazaki, Aichi 444-8585, Japan; [b]Department of Physiological Sciences, Graduate University for Advanced Studies (SOKENDAI), Hayama, Kanagawa 240-0193, Japan; [c]Department of Molecular and Cell Biology; [d]Helen Wills Neuroscience Institute, University of California, Berkeley, CA 94720; and [e]Physical Bioscience Division, Lawrence Berkeley National Laboratory, Berkeley, CA 94720

Edited* by Lily Yeh Jan, University of California, San Francisco, CA, and approved August 31, 2010 (received for review July 16, 2010)

The KCNQ1 voltage-gated potassium channel and its auxiliary subunit KCNE1 play a crucial role in the regulation of the heartbeat. The stoichiometry of KCNQ1 and KCNE1 complex has been debated, with some results suggesting that the four KCNQ1 subunits that form the channel associate with two KCNE1 subunits (a 4:2 stoichiometry), while others have suggested that the stoichiometry may not be fixed. We applied a single molecule fluorescence bleaching method to count subunits in many individual complexes and found that the stoichiometry of the KCNQ1 – KCNE1 complex is flexible, with up to four KCNE1 subunits associating with the four KCNQ1 subunits of the channel (a 4:4 stoichiometry). The proportion of the various stoichiometries was found to depend on the relative expression densities of KCNQ1 and KCNE1. Strikingly, both the voltage-dependence and kinetics of gating were found to depend on the relative densities of KCNQ1 and KCNE1, suggesting the heart rhythm may be regulated by the relative expression of the auxiliary subunit and the resulting stoichiometry of the channel complex.

GFP | single molecule fluorescence | potassium channel | subunit counting | gating

KCNQ1 is a voltage-gated K^+ (Kv) channel that is expressed in a wide variety of tissues, including human heart, pancreas, kidney, lung, inner ear, and intestine (1–3). Like other Kv channels, each KCNQ1 subunit has six transmembrane segments (S1–S6), with S1–S4 segments serving as a voltage-sensor domain, S5–S6 segments forming a pore domain and four KCNQ1 subunits forming the ion channel (4–7). One of the most prominent features of the KCNQ1 channel is that its gating is dramatically affected by the single transmembrane domain proteins encoded by the KCNE gene family. KCNE1, which is coexpressed with KCNQ1 in the heart and inner ear, drastically slows the activation and deactivation kinetics of the KCNQ1 channel and enhances current amplitude (1, 8, 9). Another KCNE family member, KCNE3, makes the KCNQ1 channel constitutively open in the intestine (3). The remaining members of the KCNE family, KCNE2, 4, and 5 reduce KCNQ1 current amplitude or modulate the gating (10–12).

Although there is little structural information about the KCNQ1 – KCNE1 complex (7, 13), KCNE1 has been shown to directly bind to the pore region of KCNQ1 (14). In addition, a functional interaction between KCNE proteins and the voltage-sensor domain of KCNQ1 has been suggested by several reports, and the interaction surfaces have been modeled and mapped by cross linking (15–20). The interaction studies suggest that KCNE1 resides between two adjacent voltage-sensor domains, at the junction with the pore region (15–20). This kind of packing would seem to be compatible with a 4:4 stoichiometry between KCNQ1 and the KCNE subunits. However, several studies concluded that only two KCNE1 subunits bind to four KCNQ1 subunits (4:2 stoichiometry) (21–23). In contrast, a study of KCNE1 – KCNQ1 fusion proteins suggested the existence of multiple stoichiometries (24).

In order to directly observe the number of KCNE1 subunits in the KCNQ1 – KCNE1 complex, we employed a single molecule imaging technique using total internal reflection fluorescence (TIRF) microscopy to image fluorescent protein (FP) tagged membrane proteins (25, 26). The proteins were expressed at low density in *Xenopus laevis* oocytes permitting individual channel complexes to be resolved as single fluorescent spots. By counting bleaching steps of the FP in each spot, we were able to count the number of subunits in each complex. We confirmed that KCNQ1 is a tetramer on the plasma membrane, as suggested by homology with Shaker-type potassium channels. When FP-tagged KCNE1 was coexpressed with KCNQ1 we observed a substantial number of complexes with three or four bleaching steps, indicating that more than two KCNE1 subunits can assemble with one KCNQ1 ion channel complex. We found that the stoichiometry is variable, and that it depends on the relative densities of KCNQ1 and KCNE1. A fusion protein of two KCNQ1 subunits to one KCNE1, which is forced to have a 4:2 stoichiometry could be further modulated by addition of free KCNE subunits, but a fusion of one KCNQ1 subunit to one KCNE1 subunit, to force a 4:4 stoichiometry, could not be further modulated by free KCNE subunits, indicating that the maximal modulation occurs at either 4:3 or at the maximal occupancy of 4:4. We consider the functional implications of high occupancy complexes.

Results

KCNQ1 Forms a Tetramer. Before investigating how many KCNE1 subunits bind to the KCNQ1 channel, we first examined the stoichiometry of channels formed by KCNQ1 alone using the single molecule subunit counting method (25). We tagged the KCNQ1 channel with monomeric enhanced green FP (mEGFP) at the C terminus (KCNQ1 – mEGFP). KCNQ1 – mEGFP expressed well in *Xenopus* oocytes and its current looked similar to normal KCNQ1 current under the two-electrode voltage clamp. Under TIRF illumination and high-sensitivity imaging, using low expression levels where individual spots of fluorescence could be resolved, most of the fluorescent spots of KCNQ1 – mEGFP were found to be mobile (Fig. S1). Because it is difficult to count photobleaching steps of mobile fluorescent spots, we hoped that a different position of the mEGFP tag would change the mobility of the KCNQ1 + mEGFP fusion construct, and moved the mEGFP tag either to the cytoplasmic N terminus (mEGFP – KCNQ1) or into a restriction enzyme NotI site in the middle of the cyto-

Author contributions: K.N., M.H.U., and E.Y.I. designed research; K.N. performed research; M.H.U. and E.Y.I. contributed new reagents/analytic tools; K.N. and M.H.U. analyzed data; and K.N., Y.K., and E.Y.I. wrote the paper.

The authors declare no conflict of interest.

*This Direct Submission article had a prearranged editor.

See Commentary on page 18751.

[1]Present address: Centre for Biological Signalling Studies (BIOSS) and Center for Biological Systems Analysis (ZBSA), Albert-Ludwigs-University Freiburg, Germany.

[2]To whom correspondence should be addressed. E-mail:ehud@berkeley.edu.

This article contains supporting information online at www.pnas.org/lookup/suppl/doi:10.1073/pnas.1010354107/-/DCSupplemental.

plasmic N-terminal domain (mEGFP$_{NotI}$KCNQ1) (Fig. 1*A*). Both mEGFP – KCNQ1 and mEGFP$_{NotI}$KCNQ1 expressed well in oocytes. Both showed wild-type KCNQ1 like voltage-dependent potassium current when expressed alone, and also showed slowly activating potassium current when expressed with KCNE1 (as shown for mEGFP$_{NotI}$KCNQ1 in Fig. S2). Most importantly, large fractions of the fluorescent spots of both mEGFP–KCNQ1 and mEGFP$_{NotI}$KCNQ1 were immobile (Fig. S1).

By adjusting the amount of RNA injected into the cells and the expression time we achieved a membrane density appropriate for counting, where multiple spots could be imaged, but the density was low enough to minimize the chance of two channels falling within the same diffraction-limited spot (20–200 spots in a 13×13 μm under TIRF illumination area) (Fig. 1*B*). About half of the fluorescent spots were immobile such that their intensity did not fluctuate due to movement perpendicular to the cover slip. We counted bleaching steps of mEGFP fluorescence in oocytes expressing either mEGFP – KCNQ1 or mEGFP$_{NotI}$KCNQ1, and observed a range of bleaching steps, with four steps being the largest number (Fig. 1 *C*, *D*). To relate these counts to the number of mEGFP-labeled subunits, one has to take into account that not every mEGFP is fluorescent and that, consequently, the distribution of bleaching steps follows a binomial distribution with a probability (p) of mEGFP being fluorescent (25). We collected 240 countable spots for mEGFP – KCNQ1 from five optical patches from one oocyte and 258 spots for mEGFP$_{NotI}$KCNQ1 from seven optical patches from one oocyte. The observed distributions were well fit by a binomial distribution with $p = 64$ and 70%, respectively (Fig. 1*D* and Fig. S3). Because some of the fluorescent spots of mEGFP – KCNQ1 and mEGFP$_{NotI}$KCNQ1 were still slightly mobile, we attempted to further immobilize the channels by adding the C-terminal domain of the Kv1.4 channel (which includes its PDZ binding motif) at the end of the C terminus of mEGFP – KCNQ1 (mEGFP–KCNQ1 – Kv1.4C) and by coexpression of a postsynaptic protein PSD-95. This strategy was used earlier to immobilize Ci-VSP (*Ciona intestinalis* voltage-sensor containing phosphatase) , without affecting the estimate of its stoichiometry (27). As was the case above, four bleaching step spots were frequently observed, and the distribution was well fit by a binomial distribution with $p = 73\%$. However, the fraction of immobile fluorescent spots was not increased by the PDZ anchoring (Fig. S1).

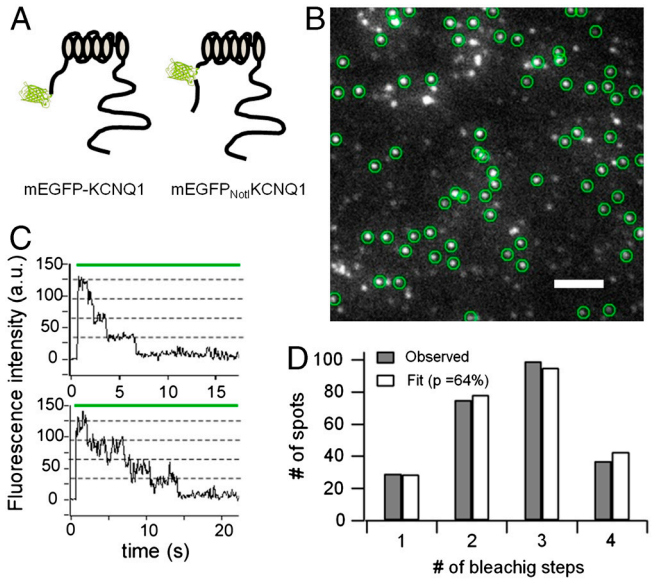

Fig. 1. KCNQ1 forms a tetramer. (*A*) Schematic diagram of mEGFP – KCNQ1 and mEGFP$_{NotI}$KCNQ1 constructs. mEGFP was inserted in the middle of the cytoplasmic N-terminal domain in mEGFP$_{NotI}$KCNQ1. (*B*) A single frame from a TIRF movie of a *Xenopus* oocyte expressing mEGFP – KCNQ1. Green circles indicate immobile spots suitable for counting. (Scale bar: 2 μm). (*C*) Examples of four bleaching steps from two spots of mEGFP – KCNQ1. Dotted lines indicate the fluorescence intensity of single mEGFPs. (*D*) Distributions of observed bleaching step numbers (gray bars) from oocytes expressing mEGFP – KCNQ1. Distribution profiles are well fit by a binomial distribution with p (probability of GFP to be fluorescent) of 64% (white bars).

With and without the added PDZ interaction domain, the observations are consistent with KCNQ1 being made of four subunits. The probability for fluorescence of the mEGFP and the frequency of counting four bleaching steps were both a little lower than what was seen earlier for several tetrameric channels (where $p = 80\%$ and the frequency of spots with three and four bleaching steps is equal) (25, 28, 29). This deviation likely reflects the endogenous *Xenopus* oocyte KCNQ1 subunit, xKCNQ1 (1), which is expected to provide unlabeled subunits to a minority of the channels. We used the value of $p = 80\%$ in our subsequent analysis (although the underestimated measured value gave the same results).

Up to Four KCNE1 Subunits per KCNQ1 Channel. Next, we set out to count the number of KCNE1 subunits in each KCNQ1 complex. For this experiment, KCNE1 was tagged at the end of its cytoplasmic C-terminal region with mEGFP (KCNE1 – mEGFP). TIRF imaging showed that KCNE1 – mEGFP alone traffics well to the cell surface. However, most of the KCNE1 – mEGFP fluorescent spots were mobile and not suitable for counting (Fig. S4, immobile fraction is 12.5%). We therefore added Kv1.4C at the end of the C-terminal domain of KCNE1 (KCNE1 – mEGFP–Kv1.4C). This addition increased the fraction of immobile fluorescent spots even without PSD-95 (Fig. S4, immobile fraction is 34.0%) and so became our construct of choice for these experiments, without added PSD-95. Voltage clamp measurements showed that KCNE1 – mEGFP – Kv1.4C is functional and modulates N-terminal monomeric red FP mCherry tagged KCNQ1 (mCherry – KCNQ1) currents in the same way as does untagged KCNE1 (Fig. S5).

KCNE1 – mEGFP – Kv1.4C was coexpressed with mCherry–KCNQ1. Oocytes were injected with 0.005 ng and 5 ng of the two RNAs, respectively, to balance surface expression density, as judged by TIRF imaging in individual injections. To image the two FP tags, we first excited and imaged red mCherry for 5 s —long enough to almost bleach it—and subsequently excited and imaged mEGFP (Fig. 2 *A*, *B* and Fig. S6). In this way we avoided a potential complication for detecting mEGFP that could arise from fluorescence resonance energy transfer from mEGFP to mCherry. To identify KCNE1 that was associated with KCNQ1 from free KCNE1, we superimposed the green and red images (Fig. 2*A* right) and identified mEGFP spots that overlapped with mCherry spots (white arrowheads in Fig. 2*A*). We collected 770 countable green spots from 22 optical patches from four oocytes of two different batches. 291 out of 770 green spots (37.8%) were overlapped with red spots. We calculated the chance that mEGFP and mCherry labeled KCNE1 and KCNQ1 would incidentally fall within a diffraction-limited spot without being associated (see *SI Text*). At the expression densities employed in the experiments, the fraction of incidental red/green colocalization (f) ranged from 1.1% to 4.9%, with an average of $2.1 \pm 0.0\%$ ($n = 22$ patches), well below the fraction of observed colocalization.

Using the previously reported 80% probability of mEGFP being fluorescent (25, 28, 29), we generated predicted distributions of bleaching steps for 1, 2, 3, and 4 KCNE1 subunits per tetrameric KCNQ1 channel (Fig. 2*C*, right). These predicted distributions were compared to the observed distribution of mEGFP bleaching steps in the red + green spots (Fig. 2*C*, left). The observed distribution was differed from each of the predicted distributions, suggesting, instead that it was a mixture of them. Thus, the results indicate that multiple KCNE1 subunits associate

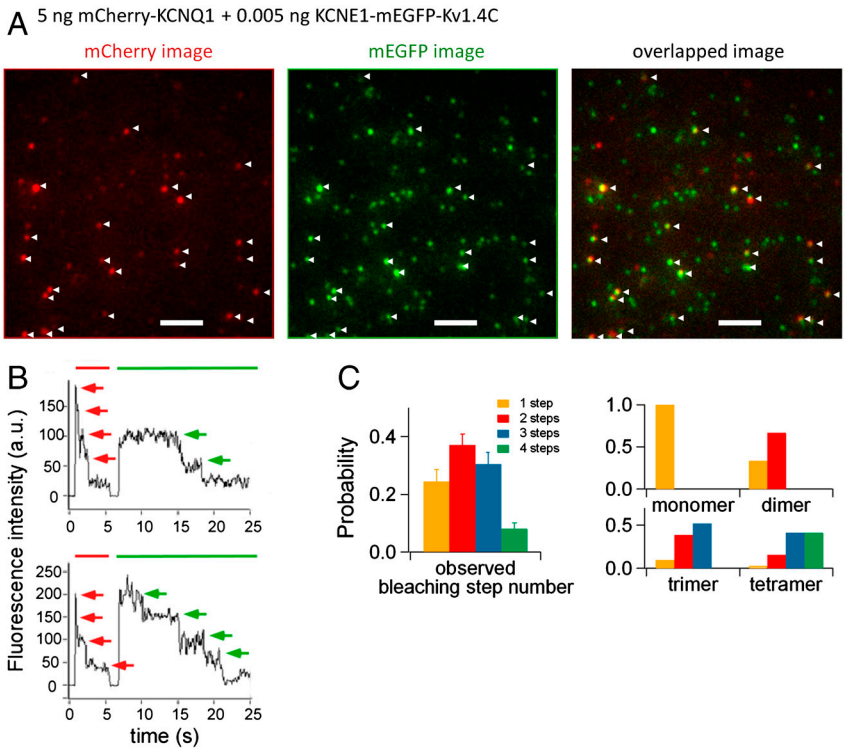

Fig. 2. Up to four KCNE1 subunits within a KCNQ1 complex. (*A*) Images from *Xenopus* oocytes coexpressing mCherry – KCNQ1 and KCNE1 – mEGFP – Kv1.4C. mCherry image (left) and mEGFP image (center) are superimposed (right). Overlapping spots are marked by white arrowheads. (Scale bars: 2 μm). (*B*) Examples of multiple bleaching steps of mEGFP fluorescence from two representative spots with both red and green fluorescence. Illumination at 593 nm to excite mCherry for 5 s (red bars) was followed by illumination at 488 nm to excite mEGFP (green bars). Top example shows two bleaching steps while bottom example shows four bleaching steps. Arrows indicate the fluorescence levels. (*C*) (Left) Observed frequency distribution of the number of mEGFP bleaching steps from the mCherry(KCNQ1) + EGFP(KCNE1) overlapping spots (mean ± sem, $n = 22$ (optical patches from four oocytes of two different batches). (Right) Theoretical probabilities for monomers, dimers, trimers, and tetramers with p (probability of mEGFP being fluorescent) = 80%.

with each KCNQ1 tetramer and suggest that the stoichiometry of KCNE1 subunits per channel may not be fixed.

We also counted the bleaching step numbers of KCNE1–mEGFP – Kv1.4C in the absence of KCNQ1. Most of the spots (124 out of 151) showed a single bleaching step, indicating that KCNE1 – mEGFP – Kv1.4C exists as a monomer on the membrane (Fig. S4*C*).

KCNQ1 – KCNE1 Stoichiometry Depends on the Relative Densities. To test the possibility, suggested above, that the number of KCNE1 subunits per channel may not be fixed, we varied the relative densities of KCNQ1 and KCNE1 and asked how this impacts the stoichiometry. To obtain a range of KCNQ1 and KCNE1 densities, we injected mCherry – KCNQ1 mRNA in a range of 0.25–25 ng and KCNE1 – mEGFP – Kv1.4C in a range of 0.005–0.025 ng (i.e., the ratio of RNAs was between 10–1,000). Because the expression density on the plasma membrane was not always uniform, even within a same oocyte, we determined the densities of the two proteins directly by counting all of the mobile and immobile fluorescent spots at the beginning of illumination for both mCherry and mEGFP within the 13×13-μm^2 area optical patch. We counted fluorescent spots from 38 optical patches from seven oocytes in four batches of oocyte isolation. From the oocytes having relatively high mCherry signal (red, orange, yellow, and yellow-green plots in Fig. 3; Group A), the number of red spots and green spots per optical patch were 177 ± 9 and 133 ± 8 respectively, yielding an mEGFP/mCherry relative density of 0.8 ± 0.0 and $f = 3.1 \pm 0.1\%$ (fraction of colocalization from randomly distributed red and green spots at this relative density; $n = 24$). From the oocytes having relatively low mCherry signal (green and blue plots in Fig. 3; Group B), the number of spots were 67 ± 13 for red spots and 139 ± 25 for green spots with a relative density of 2.2 ± 0.1 and $f = 1.9 \pm 0.0\%$ ($n = 10$). From the oocytes having high mEGFP expression (purple spots in Fig. 3; Group C), the number of spots were 98 ± 5 for red spots and 529 ± 39 for green spots with a relative density of 5.5 ± 0.4 and $f = 3.4 \pm 0.0\%$ ($n = 4$).

We counted mEGFP bleaching step numbers exclusively from spots that overlapped with red fluorescence (i.e., where the green KCNE1 colocalized with red KCNQ1). As the relative density of mEGFP/mCherry increased so did the number of bleaching steps (Fig. 3). The average number of bleaching steps was 2.1 ± 0.1 ($n = 24$; Group A), 2.5 ± 0.1 ($n = 10$; Group B), and 3.2 ± 0.1 ($n = 4$; Group C). The dotted lines in Fig. 3 indicate the expected average number of bleaching steps for pure dimer (1.7), trimer (2.4), and tetramer (3.2) for a probability of 80% that the mEGFP would be fluorescent. The results indicate that the

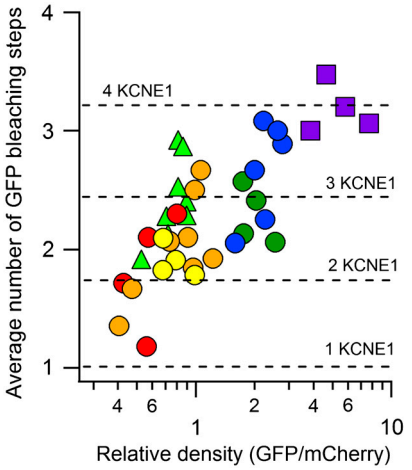

Fig. 3. Stoichiometry of the KCNQ1 : KCNE1 complex depends on the relative density of expression of KCNQ1 and KCNE1. Average number of bleaching steps of mEGFP fluorescence for each optical patch is plotted against the relative density of mEGFP (KCNE1) to mCherry (KCNQ1) in the patch. X-axis is in a logarithmic scale. Data were taken from 38 optical patches from seven oocytes of four different batches. Same color indicates multiple patches from same oocyte. The ratio of two RNAs (mCherry – KCNQ1/KCNE1–mEGFP – Kv1.4C) for the oocyte represented by the purple squares was 10, that of yellow-green triangles was 100, and the remainder (circles) were 1,000. If relative density is lower than 1, there are more red spots (KCNQ1) than green spots (KCNE1). If relative density is higher than 1, there are more KCNE1 subunits than KCNQ1. Dashed lines indicate expected values for 1–4 KCNE1 subunits if the stoichiometry is fixed.

stoichiometry of KCNQ1 : KCNE1 is variable, not fixed, and that it ranges from 4 : 1 to 4 : 4 depending on the relative densities of KCNQ1 and KCNE1.

Gating Properties of KCNQ1 – KCNE1 Current Depend on Stoichiometry. Having found that the stoichiometry of the KCNQ1–KCNE1 complex varies with the relative densities of expression, we asked whether the functional properties of the channel would reflect the differences in stoichiometry. We analyzed the electrophysiological properties of KCNQ1 – KCNE1 with various amounts of KCNE1 RNA. We injected 0.0025–7.5 ng of wild-type KCNE1 RNA along with 25 ng of wild-type KCNQ1 RNA. As KCNE1 RNA was increased the rate of activation of the current became slower and the amplitude of the current increased (Fig. 4*A*, top). Current amplitudes were largest at 0.25 ng KCNE1 RNA and then gradually decreased at higher KCNE1 RNA concentrations (Fig. 4*A*). In addition to the effect on current kinetics and amplitude, the conductance voltage (*G-V*) relations progressively shifted to the right as the amount of KCNE1 RNA was increased (Fig. 4*B*). Both the effect on current amplitude and the *G-V* shift were maximal at about 0.25 and 0.75 ng of KCNE1 RNA (Fig. 4 *A*, *B*). At even higher KCNE1 RNA current amplitude decreased, but without evident effect in gating kinetics or voltage dependence, suggesting that additional KCNE1 subunits either may compete with KCNQ1 for translation or membrane targeting.

So far, our subunit counting experiments indicate that up to four KCNE1 subunits can assemble into one KCNQ1 channel complex and our functional experiments show that as the amount of KCNE1 expression rises relative to that of KCNQ1 there is an increased functional impact up to a maximal point. However, the functional experiments in Fig. 4 required higher overall expression (more time of expression following RNA injection) to enable accurate current measurements to be made, and so could not be readily related to the subunit counting measurements in Fig. 3. We therefore designed an alternative approach to examine the functional impact of increasing the number of KCNE1 subunits from two to four. In this experiment we made a tandem construct of one KCNE1 subunit and two KCNQ1 subunits (E1 – Q1 – Q1 tandem) to mimic the 4 : 2 (Q1 : E1) channel. A similar experiment using tandem constructs by others showed that coexpression of E1 – Q1 – Q1 tandem with free KCNE1 further slows the activation kinetics of the tandem construct (24). Here we used shifts in the *G-V* curve to gauge whether additional KCNE1 subunits could be added to the complex. E1 – Q1 – Q1 (25 ng) produced a slowly activating current with a half activation voltage ($V_{1/2}$) of 47.1 ± 2.2 mV ($n = 6$). Coexpression of E1 – Q1 – Q1 (25 ng) with KCNE1 (2.5 ng) shifted the *G-V* curve to 53.9 ± 1.7 mV ($n = 6$, $P < 0.05$) (Fig. 4*C*). We also tested coexpression of KCNE3, another auxiliary subunit of KCNQ1, which boosts KCNQ1 channels by making them constitutively active (3). Interestingly, coexpression of KCNE3 (2.5 ng) with E1 – Q1 – Q1 (25 ng) significantly inhibited the current, with maximum tail current amplitudes decreasing from 2.84 ± 0.39 μA ($n = 6$) for E1 – Q1 – Q1 alone to 0.51 ± 0.07 μA ($n = 6$, $P < 0.01$) for E1 – Q1 – Q1 coexpressed with KCNE3 (Fig. 4*C*). Thus, the enhancement of channel activity by KCNE1 and KCNE3 (the former by boosting opening, although slowing the rate of opening,

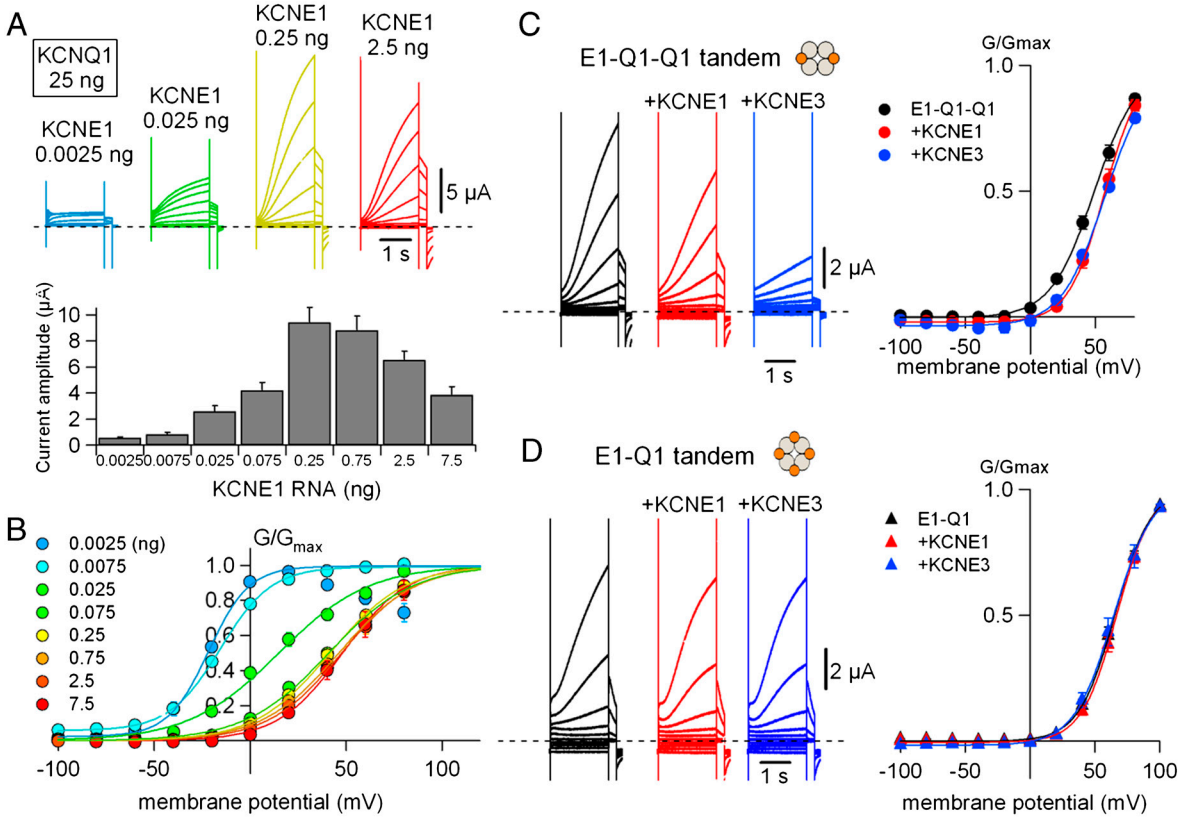

Fig. 4. Gating properties of KCNQ1 – KCNE1 complexes with different ratios of expression of KCNE1 to KCNQ1. (*A*) KCNQ1 currents with KCNE1 coexpressed at various RNA concentrations, 2 d after RNA injection. Voltages were stepped from −100 mV to various voltages (up to +80 mV) before being stepped to −30 mV for tail current measurement. Maximum tail current amplitude for each KCNE1 concentration is plotted below ($n = 6$ for each concentration). (*B*) Normalized *G-V* curves for different concentrations of KCNE1 RNA. *G-V* curves are fitted to the Boltzmann function. (*C*) Current traces and *G-V* curves of a linked construct of one KCNE1 subunit linked to two KCNQ1 subunits (the E1 – Q1 – Q1 tandem) alone (black) and coexpressed with free KCNE1 (red) or KCNE3 (blue). (*D*) Current traces and *G-V* curves of a linked construct of one KCNE1 subunit linked to one KCNQ1 subunit (the E1 – Q1 tandem) alone (black) and coexpressed with KCNE1 (red) or KCNE3 (blue).

and shifting the *G-V* to more depolarized potentials, and the latter by rendering the channel constitutively active) do not add, but counteract each other. The results indicate that either KCNE1 or KCNE3 subunits can add to 4:2 Q1:E1 channels and thereby modulate their function, i.e., that more than two KCNE subunits can assemble into a tetrameric KCNQ1 channel.

The above results and our single subunit counting suggest that four KCNE subunits may associate with one KCNQ1 channel. To test this, we made a tandem construct of one KCNE1 subunit and one KCNQ1 subunit (E1 – Q1) to force a stoichiometry of 4:4. E1 – Q1 (25 ng) produced large currents (4.57 ± 0.68 μA, maximum tail current amplitude) with slow opening kinetics, and a positively shifted *G-V* curve (65.2 ± 1.9 mV, $V_{1/2}$, $n = 6$), typical of the coassembled channel. Coinjection of either KCNE1 or KCNE3 with E1 – Q1 affected neither the current amplitude nor the *G-V* relation (Fig. 4*D*), suggesting that no additional KCNE subunits were able to join with and modulate the 4:4 Q1:E1 channel.

Taken together, our electrophysiological data support our optical observations with subunit counting that up to four KCNE1 subunits can assemble with one tetrameric KCNQ1 channel, with the number dependent on the relative density of expression of the channel forming and auxiliary subunits. Moreover, the data argue that as the number of KCNE1 subunits increases so does the strength of the modulation, but that the nature of the modulation by different KCNEs can be sufficiently different so that their mixture results have unpredictable outcomes for function.

Discussion

The stoichiometry of the KCNQ1 – KCNE1 complex has been a matter of extended debate. Because K^+ channels that are made of four identical subunits are structurally symmetrical (5, 30–32), one might imagine that there would be four identical docking sites for the modulatory subunit. However, some homotetrameric channels, such as ionotropic glutamate receptors (33), have ligand binding domains that function as dimers of dimers, breaking the fourfold symmetry and providing a scaffold that could, in principle, provide for docking of only two modulatory subunits. Moreover, even in the case of a fourfold symmetric channel, it is possible that the association with a modulatory subunit would alter the channel structure so that some of the binding sites would become unavailable. Indeed, several recent studies have concluded that the KCNQ1 channel, which we confirm to be homotetrameric, has a fixed 4:2 stoichiometry with its modulatory KCNE subunits (21–23). However, contradictory evidence has also been published in support of a multiple stoichiometry model (24).

Our single molecule subunit counting experiments show that the number of KCNE subunits per channel can vary from one to four, depending on the relative expression levels of the channel forming KCNQ1 subunit and the modulatory KCNE subunit (Fig. 5). How then could one account for the studies that supported a 4:2 stoichiometry? Two of those studies (21, 22) attempted to deduce the subunit ratio from macroscopic currents that our experiments suggest reflected a mixture of stoichiometries, which would have been difficult to distinguish. The third study concluded that two KCNE1 subunits exist in the complex based on the effect of conjugation of cysteine-reactive tethered charybdotoxin (23). However, the functional assay for these experiments used test pulses to +20 mV, which is only at the foot of the *G-V* of the 4:4 channel (Fig. 4 *B*, *D*) so that the majority of the current that they analyzed could have come from 4:2 channels.

Our functional assays indicate that the modulatory gating effects of KCNE1 on the KCNQ1 channel become larger as more KCNE1 subunits join the complex, up to when there are four KCNE1 subunits per tetrameric KCNQ1 channel (the 4:4 stoichiometry). This gating property agrees with earlier work

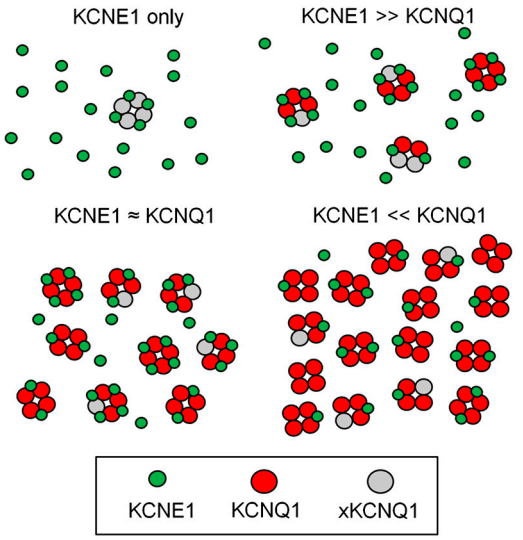

Fig. 5. Model of density-dependent stoichiometry of the KCNQ1 – KCNE1 complex. Stoichiometry of the KCNQ1 – KCNE1 complex depends on how many free KCNE1 subunits (green circles) are available for the exogenous KCNQ1 channels (red circles). Endogenous KCNQ1 subunits (xKCNQ1) in *Xenopus* oocytes are depicted as gray circles. Because we could not count xKCNQ1 and do not know if xKCNQ1 forms heteromultimers with human KCNQ1, the behavior of xKCNQ1 is unknown. However, the smaller value of *p* (probability of fluorescent GFP) shown in Fig. 1 suggests the involvement of xKCNQ1 subunit in human KCNQ1 channel.

by Romey et al. (34), who developed a kinetic model for such a density-dependent stoichiometry. Interestingly, we find that the additional effect of adding KCNE subunits to channels forced by tandem construction to already have two is small (Fig. 4*C*), indicating that the cardiac channel may be formed at ratios of KCNQ1 to KCNE1 that yield stoichiometries of 4:2 or above.

The combined impact of filling the KCNQ1 channel with four KCNE1 subunits is to slow activation and positively shift the *G-V* would tend to reduce the amount of current generated by the channels (despite the boosting effect on maximal current amplitude) because only an action potential would be depolarizing enough to reach the foot of the *G-V*, and it would be so short lived as to produce little channel activation. As a result, the 4:4 KCNE1:KCNQ1 stoichiometry channel may be selectively sensitive to trains of action potentials, while channels with no KCNE1 or fewer KCNE1 subunits are expected to respond to smaller and shorter depolarizations. The impact of such modulation is seen in *Xenopus* embryos, where KCNQ1 – KCNE1 current is involved in early left-right patterning (35), overexpression of KCNE1 affects the differentiation of the embryonic stem cells because of the shift in the *G-V* (36).

In recent years, the existence of a three subunit complex of KCNQ1 – KCNE1 – KCNE*x* (where $x = 2$, 3, or 4) has been reported (37–39). Our results indicate that addition of the other KCNE subunits, such as KCNE3, to a complex of KCNQ1 with fewer than four KCNE1 subunits, could substantially inhibit the current. Not only could modulatory subunit addition take place during channel assembly in endoplasmic reticulum or Golgi (40, 41) to create stable stoichiometries that last for the lifetime of the channel, but it may also occur on the cell surface (42, 43). Our results indicate that KCNE1 subunits can be transported to the plasma membrane by themselves and that, at high expression levels, they can be found on their own, not colocalized with KCNQ1 (Fig. 2*A*). These free KCNE1 proteins might be able to dock in vacant binding sites of KCNQ1 channels. Indeed, injection into oocytes of KCNE1 or KCNE3-containing lipid vesicles has been shown to deliver them to the surface membrane

of *Xenopus* oocyte where they modulate preexpressed KCNQ1 channels (43, 44).

In conclusion, our results show that the number of KCNE subunits associated with a KCNQ1 channel can vary from one to four, with different stoichiometries having distinct gating properties.

Materials and Methods

Molecular Biology. Human KCNQ1 (AF000571), rat KCNE1 (NM_012973), and mouse KCNE3 (NM_020574) cDNAs were subcloned into the pGEMHE expression vector. For KCNQ1, mEGFP and mCherry were fused to the N-terminal end with a flexible linker (GGSGGSGGSGGSGGRS) (25) (mEGFP – KCNQ1), or amplified by PCR and inserted into the NotI site (Arg82) of the cytoplasmic N-terminal region ($mEGFP_{NotI}KCNQ1$). The Kv1.4 C terminus (amino acids 586–654) was fused to the end of C terminus of mEGFP – KCNQ1 making the mEGFP – KCNQ1 – Kv1.4C construct. For rat KCNE1, mEGFP was fused to the C-terminal end with a flexible linker (SRGTSGGSGGSRGSGGSGG). The Kv1.4 C terminus (amino acids 586–654) was fused to the end of mEGFP making the final KCNE1 – mEGFP – Kv1.4C construct. Tandem fusion proteins of KCNE1 – KCNQ1 – KCNQ1 (E1 – Q1 – Q1) and KCNE1 – KCNQ1 (E1 – Q1) were made by PCR with a flexible linker (SRGGSGGSGGSGGSGGRS). All constructs were confirmed by DNA sequencing. RNA was transcribed using T7 mMessage mMachine Kit (Ambion).

Optical and Gating Measurements. For details on methods of single molecule counting, determination of stoichiometry, calculation of fractional colocalization, electrophysiology and gating analysis see *SI Text*.

ACKNOWLEDGMENTS. We thank S. Wiese and Y. Asai for valuable technical assistance. We thank T. Takumi (Hiroshima University) for the cDNA of rat KCNE1 and T. Hoshi (University of Pennsylvania) for the cDNA of human KCNQ1 channel. This work was supported by research grants from the Ministry of Education, Culture, Sports, Science, and Technology of Japan (20790184 to K.N.) and the National Institutes of Health (R01 NS35549 to E.Y.I).

1. Sanguinetti MC, et al. (1996) Coassembly of K_VLQT1 and minK (IsK) proteins to form cardiac I_{Ks} potassium channel. *Nature* 384:80–83.
2. Neyroud N, et al. (1997) A novel mutation in the potassium channel gene KVLQT1 causes the Jervell and Lange-Nielsen cardioauditory syndrome. *Nat Genet* 15:186–189.
3. Schroeder BC, et al. (2000) A constitutively open potassium channel formed by KCNQ1 and KCNE3. *Nature* 403:196–199.
4. Long SB, Campbell EB, Mackinnon R (2005) Voltage sensor of Kv1.2: structural basis of electromechanical coupling. *Science* 309:903–908.
5. Long SB, Campbell EB, Mackinnon R (2005) Crystal structure of a mammalian voltage-dependent Shaker family K^+ channel. *Science* 309:897–903.
6. Long SB, Tao X, Campbell EB, MacKinnon R (2007) Atomic structure of a voltage-dependent K^+ channel in a lipid membrane-like environment. *Nature* 450:376–382.
7. Smith JA, Vanoye CG, George AL, Jr, Meiler J, Sanders CR (2007) Structural models for the KCNQ1 voltage-gated potassium channel. *Biochemistry* 46:14141–14152.
8. Takumi T, Ohkubo H, Nakanishi S (1988) Cloning of a membrane protein that induces a slow voltage-gated potassium current. *Science* 242:1042–1045.
9. Barhanin J, et al. (1996) K_VLQT1 and IsK (minK) proteins associate to form the I_{Ks} cardiac potassium current. *Nature* 384:78–80.
10. Tinel N, Diochot S, Borsotto M, Lazdunski M, Barhanin J (2000) KCNE2 confers background current characteristics to the cardiac KCNQ1 potassium channel. *Embo J* 19:6326–6330.
11. Angelo K, et al. (2002) KCNE5 induces time- and voltage-dependent modulation of the KCNQ1 current. *Biophys J* 83:1997–2006.
12. Grunnet M, et al. (2002) KCNE4 is an inhibitory subunit to the KCNQ1 channel. *J Physiol* 542:119–130.
13. Kang C, et al. (2008) Structure of KCNE1 and implications for how it modulates the KCNQ1 potassium channel. *Biochemistry* 47:7999–8006.
14. Melman YF, Um SY, Krumerman A, Kagan A, McDonald TV (2004) KCNE1 binds to the KCNQ1 pore to regulate potassium channel activity. *Neuron* 42:927–937.
15. Nakajo K, Kubo Y (2007) KCNE1 and KCNE3 stabilize and/or slow voltage sensing S4 segment of KCNQ1 channel. *J Gen Physiol* 130:269–281.
16. Panaghie G, Abbott GW (2007) The role of S4 charges in voltage-dependent and voltage-independent KCNQ1 potassium channel complexes. *J Gen Physiol* 129:121–133.
17. Rocheleau JM, Kobertz WR (2008) KCNE peptides differently affect voltage sensor equilibrium and equilibration rates in KCNQ1 K^+ channels. *J Gen Physiol* 131:59–68.
18. Shamgar L, et al. (2008) KCNE1 constrains the voltage sensor of Kv7.1 K^+ channels. *PLoS One* 3:e1943.
19. Xu X, Jiang M, Hsu KL, Zhang M, Tseng GN (2008) KCNQ1 and KCNE1 in the I_{Ks} channel complex make state-dependent contacts in their extracellular domains. *J Gen Physiol* 131:589–603.
20. Chung DY, et al. (2009) Location of KCNE1 relative to KCNQ1 in the I_{KS} potassium channel by disulfide cross-linking of substituted cysteines. *Proc Natl Acad Sci USA* 106:743–748.
21. Wang KW, Goldstein SA (1995) Subunit composition of minK potassium channels. *Neuron* 14:1303–1309.
22. Chen H, Kim LA, Rajan S, Xu S, Goldstein SA (2003) Charybdotoxin binding in the I_{Ks} pore demonstrates two MinK subunits in each channel complex. *Neuron* 40:15–23.
23. Morin TJ, Kobertz WR (2008) Counting membrane-embedded KCNE beta-subunits in functioning K^+ channel complexes. *Proc Natl Acad Sci USA* 105:1478–1482.
24. Wang W, Xia J, Kass RS (1998) MinK-KvLQT1 fusion proteins, evidence for multiple stoichiometries of the assembled IsK channel. *J Biol Chem* 273:34069–34074.
25. Ulbrich MH, Isacoff EY (2007) Subunit counting in membrane-bound proteins. *Nat Methods* 4:319–321.
26. Ulbrich MH, Isacoff EY (2008) Rules of engagement for NMDA receptor subunits. *Proc Natl Acad Sci USA* 105:14163–14168.
27. Kohout SC, Ulbrich MH, Bell SC, Isacoff EY (2008) Subunit organization and functional transitions in Ci-VSP. *Nat Struct Mol Biol* 15:106–108.
28. Tombola F, Ulbrich MH, Isacoff EY (2008) The voltage-gated proton channel Hv1 has two pores, each controlled by one voltage sensor. *Neuron* 58:546–556.
29. Yu Y, et al. (2009) Structural and molecular basis of the assembly of the TRPP2/PKD1 complex. *Proc Natl Acad Sci USA* 106:11558–11563.
30. Jiang Y, et al. (2002) Crystal structure and mechanism of a calcium-gated potassium channel. *Nature* 417:515–522.
31. Jiang Y, et al. (2003) X-ray structure of a voltage-dependent K^+ channel. *Nature* 423:33–41.
32. Doyle DA, et al. (1998) The structure of the potassium channel: molecular basis of K^+ conduction and selectivity. *Science* 280:69–77.
33. Sobolevsky AI, Rosconi MP, Gouaux E (2009) X-ray structure, symmetry, and mechanism of an AMPA-subtype glutamate receptor. *Nature* 462:745–756.
34. Romey G, et al. (1997) Molecular mechanism and functional significance of the MinK control of the KvLQT1 channel activity. *J Biol Chem* 272:16713–16716.
35. Morokuma J, Blackiston D, Levin M (2008) KCNQ1 and KCNE1 K^+ channel components are involved in early left-right patterning in *Xenopus laevis* embryos. *Cell Physiol Biochem* 21:357–372.
36. Morokuma J, et al. (2008) Modulation of potassium channel function confers a hyperproliferative invasive phenotype on embryonic stem cells. *Proc Natl Acad Sci USA* 105:16608–16613.
37. Morin TJ, Kobertz WR (2007) A derivatized scorpion toxin reveals the functional output of heteromeric KCNQ1 – KCNE K^+ channel complexes. *ACS Chem Biol* 2:469–473.
38. Toyoda F, Ueyama H, Ding WG, Matsuura H (2006) Modulation of functional properties of KCNQ1 channel by association of KCNE1 and KCNE2. *Biochem Biophys Res Commun* 344:814–820.
39. Manderfield LJ, George AL, Jr (2008) KCNE4 can coassociate with the I_{Ks} (KCNQ1 – KCNE1) channel complex. *Febs J* 275:1336–1349.
40. Krumerman A, et al. (2004) An LQT mutant minK alters KvLQT1 trafficking. *Am J Physiol Cell Ph* 286:C1453–1463.
41. Chandrasekhar KD, Bas T, Kobertz WR (2006) KCNE1 subunits require coassembly with K^+ channels for efficient trafficking and cell surface expression. *J Biol Chem* 281:40015–40023.
42. Poulsen AN, Klaerke DA (2007) The KCNE1 beta-subunit exerts a transient effect on the KCNQ1 K^+ channel. *Biochem Biophys Res Commun* 363:133–139.
43. Jiang M, et al. (2009) Dynamic partnership between KCNQ1 and KCNE1 and influence on cardiac I_{Ks} current amplitude by KCNE2. *J Biol Chem* 284:16452–14662.
44. Kang C, Vanoye CG, Welch RC, Van Horn WD, Sanders CR (2010) Functional delivery of a membrane protein into oocyte membranes using bicelles. *Biochemistry* 49:653–655.